

Photoluminescent Complexes

Phosphorescent Cyclometalated Platinum(II) aNHC Complexes

Johannes Soellner and Thomas Strassner*^[a]

Abstract: The synthesis and characterization of the first bidentate C[∧]C* cyclometalated platinum(II) complexes based on abnormal *N*-heterocyclic carbenes (aNHC) is presented. The aNHC ligand precursors are prepared from benzonitriles and anilines to form 1,2,3-trisubstituted imidazolium salts. The title compounds were synthesized by in situ generation of the silver carbene complex, followed by transmetalation to platinum and subsequent introduction of the β-diketonate ligand. Structural characterization by 2D NMR experi-

ments, as well as solid-state structures unequivocally prove the abnormal binding mode of the aNHC ligands. Additionally, the photophysical properties of the platinum(II) complexes were examined and studied in detail by DFT calculations and cyclic voltammetry experiments. The title compounds proved to be strongly emissive at room temperature in the green to orange region of the visible spectrum, with emission efficiencies of up to 69%.

Introduction

The discovery of a stable *N*-heterocyclic carbene (NHC) by Arduengo and co-workers^[1] has been a turning point in organometallic chemistry. A ligand class that lay dormant for many years since the pioneering work by Wanzlick and Öfele,^[2] became a viable alternative in the synthesis of transition-metal complexes. As they attracted more and more interest of the scientific community, NHCs soon proved to be able to compete with then established ligands like phosphines, surpassing them in terms of chemical stability.^[3]

Transition-metal compounds are well known for their remarkable photophysical properties.^[4] Due to the strong spin-orbit coupling^[5] induced by the metal center, these complexes can theoretically reach luminescence efficiencies as high as 100%.^[6] In this context, especially iridium(III)-^[7] and platinum(II)-based^[8] motifs bearing cyclometalated ligands have shown promising results. We and others^[7–9] were able to show the benefits of incorporating *N*-heterocyclic carbenes as neutral donors in such systems, resulting in highly efficient emitters (Figure 1).^[9a,10] The choice of the appropriate *N*-heterocyclic carbene in combination with the introduction of other heteroatoms or functional groups to the aromatic system of the cyclometalated ligand allows a fine-tuning of the emission color and other photophysical properties. In combination with β-diketonate ligands, charge-neutral complexes with excellent

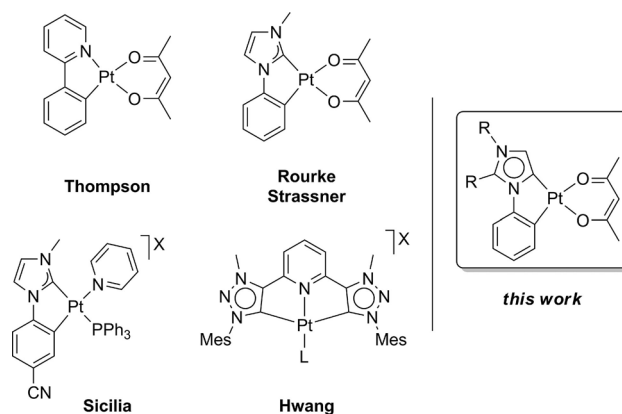



Figure 1. Selected cyclometalated Pt^{II} complexes for the application as phosphorescent emitters.

thermal stability and solubility can be synthesized which is beneficial for an application in phosphorescent organic light emitting diodes (PhOLEDs) and their assembly by vapor deposition techniques.

While the effect of normal *N*-heterocyclic carbenes on the properties of triplet emitters is relatively well understood, the impact of the abnormal binding mode (aNHC) of imidazole-based carbenes discovered in 2001^[11] remains rather unheeded.^[12] The reported higher donor strength^[13] of these mesoionic ligands compared to their classic analogues should help to further destabilize metal centered electronic states which contribute to radiationless relaxation processes of the excited molecule.^[6b] Shifting these levels to higher energies consequently reduces their accessibility, which should lead to higher quantum yields. Only very recently, related mesoionic ligands based on 1,2,3-triazoles, which rank in between imidazole based normal NHCs and aNHCs regarding their donor ability,^[14] have been applied in luminescent transition metal compounds.^[10c,15]

[a] J. Soellner, Prof. Dr. T. Strassner
Physikalische Organische Chemie
Technische Universität Dresden
01069 Dresden (Germany)
Fax: (+49) 351-463-39679
E-mail: thomas.strassner@chemie.tu-dresden.de

 Supporting information and the ORCID identification number(s) for the author(s) of this article can be found under:
<https://doi.org/10.1002/chem.201802725>

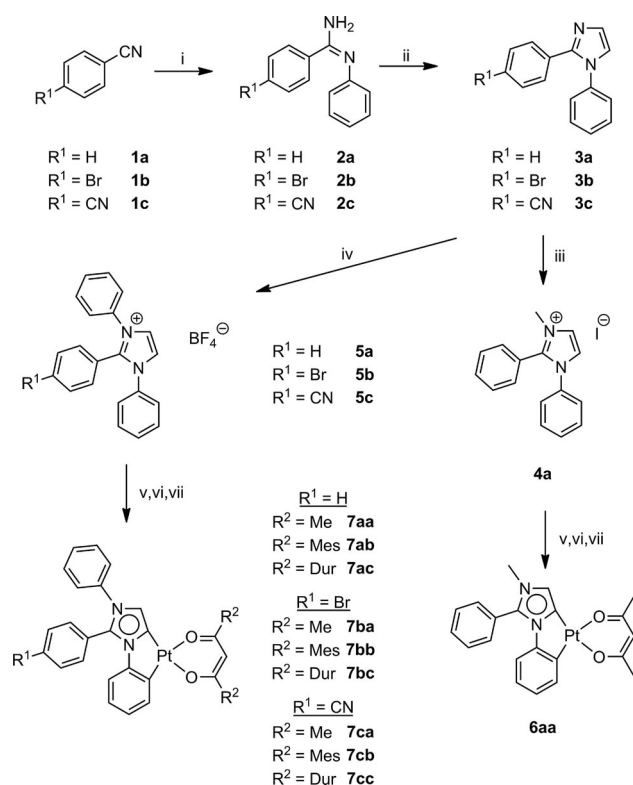
Here, we present the first examples of C^ΛC* cyclometalated platinum(II) complexes with bidentate, abnormally bound imidazolynilidene ligands.^[16] Following our studies on mesoionic 1,2,3-triazolylidenes in platinum triplet emitters^[15a] we extended our research towards the photophysics of platinum aNHC complexes.

Results and Discussion

Synthesis

Since the formation of an abnormal carbene formally involves abstraction of a proton of lower acidity compared to the one in the classic carbene position, ligand design must be adapted accordingly. To avoid side reactions during the metalation sequences, a 2-substituted imidazole motif was chosen to serve as ligand precursor. Literature shows that a blocking group, which is stable against oxidation, is desirable in this position, which is why an aryl group was selected.^[17] Amidines **2a–2c** are generated from the respective benzonitriles **1a–1c** and aniline according to a modified literature procedure using sodium hydride as base (Scheme 1).^[18] The raw products are precipitated by addition of water to the reaction mixture in DMSO. The solids are then triturated with isohexanes to yield the analytically pure *N*-arylbenzamidines **2a–2c**. Chloroacetaldehyde is used in the subsequent ring-closing step for a condensation reaction between the carbonyl group and the amine

function followed by a nucleophilic substitution of the chlorine by the imine nitrogen. The 2-substituted imidazoles **3a–3c** are then isolated by flash column chromatography. This synthetic route to 1,2-diaryl-1*H*-imidazoles offers structural variability by choice of the appropriate nitriles and anilines while also being scalable to bigger batch sizes. Ligand precursors **4a**^[19] and **5a–5c**^[20] were obtained by quaternization of imidazoles **3a–3c** with either an alkylating (**4a**) or arylating (**5a–5c**) agent (Scheme 1). The methyl-substituted compound **4a** is obtained by stirring **3a** with methyl iodide at elevated temperatures resulting in the respective iodide salt. Arylation of imidazoles **3a–3c**, to yield the respective 1,2,3-triarylimidazoles **5a–5c**, is conducted by copper(II)-catalysis using the hypervalent diphenyliodonium tetrafluoroborate salt, which was synthesized according to a known procedure.^[21] Synthesis of the metal complexes was achieved by following a modified procedure developed in our group.^[9a] This synthesis involves the in situ generation of a silver(I) carbene complex by reaction of the imidazolium salts **4a** and **5a–5c** with silver(I) oxide. Due to the lower acidity of the backbone protons, this step needs to be carried out at elevated temperatures. The ligand is then transmetalated to Pt(COD)Cl₂ (COD = 1,5-cyclooctadiene), followed by cyclometalation. The desired auxiliary ligand is introduced by addition of the appropriate β-diketone/base combination. For acetylacetonate (acac), potassium carbonate proved sufficient to deprotonate the ligand while for the mesityl (mes = 2,4,6-trimethylphenyl) and duryl (dur = 2,3,5,6-tetramethylphenyl) substituted β-diketones potassium *tert*-butoxide had to be used.



Scheme 1. Synthesis of ligand precursors and Pt^{II} complexes from substituted benzonitriles. (i) PhNH₂, NaH, DMSO, 0 °C to RT. (ii) ClCH₂CHO, CHCl₃, 70 °C. (iii) MeI, THF, 110 °C. (iv) Ph₂IBF₄, Cu(OAc)₂ × H₂O, DMF, 100 °C. (v) Ag₂O, DMF, 75 °C. (vi) Pt(COD)Cl₂, RT to 125 °C. (vii) β-diketone, base, RT to 100 °C.

Structural characterization

All complexes were characterized by standard NMR techniques and elemental analysis. All platinum complexes were additionally investigated by ¹⁹⁵Pt NMR and for all acetylacetonate complexes various 2D NMR experiments (COSY, HSQC, HMBC and NOESY) were carried out to allow for a full signal assignment.

In the ¹H NMR experiment, signals above 8 ppm are found for the protons in the backbone of the heterocycle of ligand precursors **4a** and **5a–5c**. The presence of a single-proton singlet in the aromatic region in the ¹H NMR spectra of the platinum complexes indicates deprotonation in the backbone of the heterocycle and the formation of a carbene. A characteristic ¹H–¹⁹⁵Pt hetero coupling, observed in both proton and platinum NMR, further confirms cyclometalation into the adjacent, *N*-bound phenyl ring. In the acetylacetonate complexes, ¹³C carbene resonances could be unequivocally assigned by 2D NMR to be in the range of 132 and 134 ppm, while ¹⁹⁵Pt signals for all platinum-containing compounds are observed between $\delta = -3307$ and $\delta = -3377$ ppm. Interestingly, these values are similar to those recorded for C^ΛC*-cyclometalated platinum(II) complexes with normal NHCs and β-diketone ligands.^[9a] When comparing the acetylacetonate complexes, a distinct trend in the chemical shifts of the ¹³C carbene resonances is observed, according to the electron-withdrawing ability of the substituent of the carbon-bound phenyl ring. While complexes **6aa** and **7aa** show very similar resonances at

132.1 ppm (**6aa**) and 132.3 ppm (**7aa**), a distinct shift to 133.0 (**7ba**) and 134.0 (**7ca**) is recorded for the substituted analogues, highlighting the remote influence of the substituents. This trend is in agreement with the ^{195}Pt NMR shifts measured for these complexes: the introduction of a bromine-substitution in **7ba** ($\delta(^{195}\text{Pt}) = 3375$ ppm) leads to a minor upfield shift of approximately 4 ppm when compared to the unsubstituted complex **7aa** ($\delta(^{195}\text{Pt}) = 3371$ ppm), while the influence is strongest in the nitrile-substituted complex, with **7ca** reaching a value of $\delta(^{195}\text{Pt}) = 3378$ ppm. The general trend is reproduced when comparing the complexes with either mesityl or duryl β -diketonates.

Confirmation of the proposed molecular structure was achieved by solid-state structure determination. Single crystals of **7aa** and **7ca** were grown by slow diffusion of diethyl ether and *n*-pentane into a concentrated solution of the respective compound in dichloromethane. Both aNHC platinum(II) complex crystallize in the monoclinic space group $P2_1/n$ with the unit cell containing four molecules each (Figures 2 and Figure 3). Both crystal structures are very similar and show comparable values for all characteristic bond lengths and

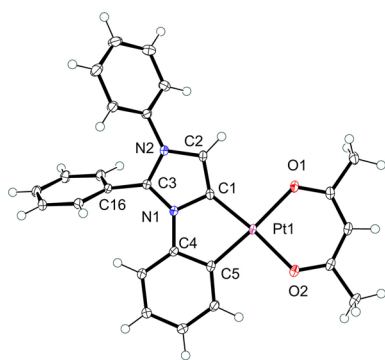


Figure 2. ORTEP3 illustration of solid-state structure of compounds **7aa**. Thermal ellipsoids at 50% probability. Selected bond lengths [Å] and angles [°]: Pt(1)–C(1) 1.9399(15), Pt(1)–C(5) 1.9673(14), Pt(1)–O(1) 2.0937(11), Pt(1)–O(2) 2.0642(11); C(1)–Pt(1)–C(5) 80.97(6), O(1)–Pt(1)–O(2) 90.47(5); O(1)–Pt(1)–C(1)–C(2) 4.3(2), C(1)–N(2)–C(4)–C(5) –2.0(2), C(1)–N(2)–C(3)–C(16) 167.2(1).

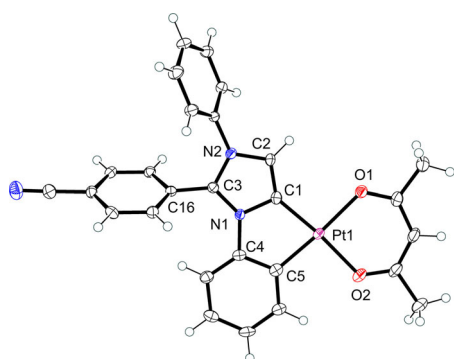


Figure 3. ORTEP3 illustration of solid-state structure of compounds **7ca**. Thermal ellipsoids at 50% probability. Selected bond lengths [Å] and angles [°]: Pt(1)–C(1) 1.954(3), Pt(1)–C(5) 1.973(3), Pt(1)–O(1) 2.098(2), Pt(1)–O(2) 2.061(2); C(1)–Pt(1)–C(5) 80.84(5), O(1)–Pt(1)–O(2) 90.52(9); O(1)–Pt(1)–C(1)–C(2) 2.0(4), C(1)–N(2)–C(4)–C(5) 3.0(4), C(1)–N(2)–C(3)–C(16) –179.0(3).

angles. The results are discussed in detail for complex **7aa**. The platinum center forms a slightly distorted square-planar coordination geometry (Figure 2). Due to the formation of a five-membered platinacycle with the carbene ligand, the C(1)–Pt(1)–C(5) angle is contracted to 80.97(6)°, while the β -diketonate ligand allows for an O(1)–Pt(1)–O(2) angle of 90.47(5)°. In the solid state the acetylacetonate is slightly twisted out of plane, displayed by the dihedral angle O(1)–Pt(1)–C(1)–C(2), while the $\text{C}^{\wedge}\text{C}^*$ cyclometalated ligand remains almost perfectly in the coordination plane. Values for Pt–C and Pt–O bonds are within the expected range and comparable to structurally related motifs featuring classic *N*-heterocyclic carbenes.^[9a] Noticeably, the carbon–carbon bond to the C-bound phenyl substituent in **7aa** is not in plane with the rest of the heterocycle, which shows up in the dihedral angle for C(1)–N(2)–C(3)–C(16). The molecular packing in the solid-state reveals no possibility for direct Pt–Pt interaction. The shortest interatomic distance is found to be 5.53 Å, which is well above their van der Waals radii. The molecular alignment is best visible in the unit cell of complex **7ca**. In both structures, the molecules form pairs of two, oriented face to face (Figure S1). These pairs align offset to each other and with different tilt angles in both solid-state structures.

Photophysical characterization

To investigate the photophysical properties of this novel class of compounds, absorption and emission spectra, as well as quantum yield, color coordinates and luminescence lifetimes at room temperature were recorded for all presented complexes.

Absorption measurements were conducted in dichloromethane solutions with an analyte concentration of $5 \times 10^{-5} \text{ mol L}^{-1}$. All complexes show relatively unstructured absorption spectra in the range of 225–450 nm (Figure 4). Common for all compounds is a low energy absorption band whose position is dependent on the substitution at the *N*-heterocyclic ligand. Upon change of the substituent at N2 from

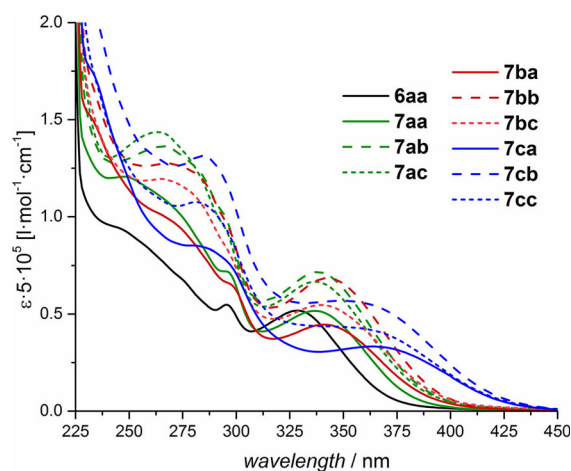


Figure 4. Quantitative UV/Vis absorption spectra for all title compounds in $5 \times 10^{-5} \text{ mol L}^{-1}$ dichloromethane solutions at room temperature.

methyl to phenyl, the band exhibits a bathochromic shift from 328 nm (**6aa**) to 337 nm (**7aa**). The band maximum further shifts for the bromine (341 nm for **7ba**) and most significantly for the nitrile substituted compounds (364 nm for **7ca**). The aryl substitutions on the β -diketonates on the other hand induce no energetic change in the transitions. Additionally, all acac complexes show a narrow band at around 295 nm that is lost or broadened in the complexes with aryl substituted β -diketonates. The assignment of these bands to orbital transitions was achieved by density functional theory (DFT) calculations (vide infra).

Poly(methyl methacrylate) (PMMA) films of all title compounds with an emitter load of 2 wt% were prepared for room temperature photoluminescence (PL) measurements (for solution PL data see Table S1). We focus on the analysis of the emissive behavior in solid state matrices, since they resemble the amorphous environment of a PhOLED more closely than solutions.^[6b] A more detailed discussion on the employed host material can be found elsewhere.^[22] In PMMA, all complexes show strong luminescence in the green-to-yellow region of the visible spectrum, with photoluminescence quantum yields (PLQY) ranging from 40 to 69% and values between 27 μ s (**7bb**) and 57 μ s (**6aa**) for the phosphorescence decay time τ_0 (Table 1).

	Φ [%] ^[a]	λ_{em} [nm] ^[b]	CIE x_1y_1 ^[c]	τ_v [μ s] ^[d]	τ_0 [μ s] ^[e]
6aa	55	545	0.389; 0.533	27	57
7aa	60	548	0.402; 0.536	22	37
7ab	58	523	0.326; 0.493	17	29
7ac	54	538	0.348; 0.499	19	35
7ba	55	558	0.429; 0.530	22	39
7bb	69	543	0.373; 0.510	19	27
7bc	53	548	0.394; 0.514	21	39
7ca	40	585	0.506; 0.482	19	47
7cb	47	571	0.483; 0.492	18	39
7cc	50	578	0.491; 0.491	18	36

[a] PLQY at room temperature and $\lambda_{exc} = 360$ nm. [b] Emission wavelength with maximum intensity at room temperature. CIE color coordinates. [d] Experimental emission lifetime. [e] τ_0 given as $\tau_0 = \tau_v / \Phi$.

The obtained spectra for the acac and mesacac complexes are given in Figure 5 (for spectra of duracac complexes see Figures S2–S4). All title compounds produce unstructured emission bands with emission maxima between $\lambda_{em} = 523$ nm (**7ab**) and 585 nm (**7ca**). The emission color is again strongly dependent on the substitution pattern of both ligands. While the replacement of the *N*-methyl group of **6aa** with a phenyl ring in **7aa**, increases the PLQY slightly from 55 to 60%, the emission spectra are nearly congruent. Aside from that all other structural variations lead to distinct changes in the emission color. Comparing only the acac complexes, the introduction of a bromine substitution in **7ba** redshifts the emission by 10 nm to $\lambda_{em} = 558$ nm, while the introduced nitrile function in **7ca** induces a bathochromic shift of 37 nm to $\lambda_{em} = 585$ nm, with re-

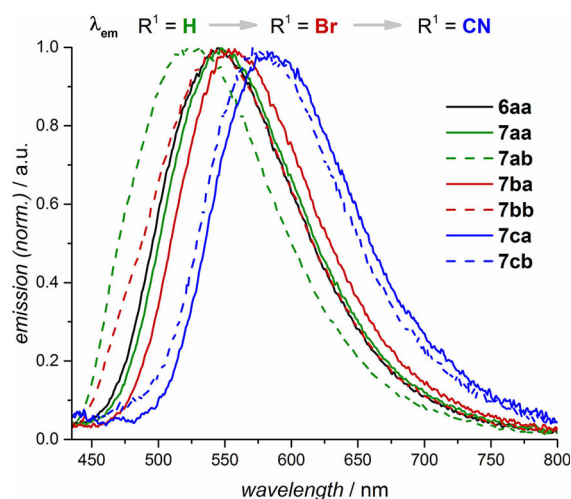


Figure 5. Emission spectra for selected title compounds in a PMMA matrix (2 wt% emitter load, $\lambda_{exc} = 360$ nm) at room temperature.

spect to **7aa**. The stronger effect on the emissive behavior of the cyano substitution is due to its higher electron-withdrawing ability, which is in accordance with the NMR shifts, discussed earlier. Another observed effect involves the different β -diketonate ligands used in this study. Changing the acac ligand to a mesityl or duryl substituted β -diketonate leads to a hypsochromic shift which is in the range of approximately 10–15 nm for most complexes.

The absence of vibrational structures in the room temperature is characteristic of metal-to-ligand charge-transfer (MLCT) involvement in the emissive process. To prove this hypothesis, emission spectra of acac containing compounds **6aa**, **7aa**, **7ba** and **7ca** were recorded at 77 K. As can be seen in Figure 6, the unstructured emission band shape is retained for all examined compounds even at low temperatures, accompanied by a hypsochromic shift (see Table S1).

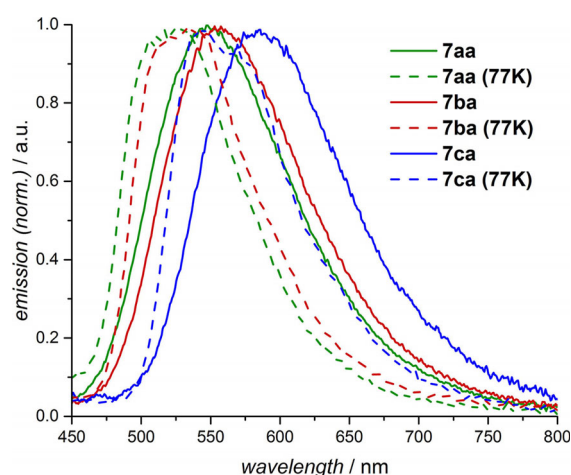


Figure 6. Comparison of emission spectra for complexes **7aa**, **7ba** and **7ca** at room temperature (2 wt% emitter in PMMA) vs. spectra at 77 K (4.5×10^{-5} mol L⁻¹ in 2-MeTHF).

DFT calculations

To better understand the photophysical processes in the presented platinum(II) complexes, DFT calculations using the Gaussian16 program package were used.

Different functional-basis set combinations involving the GGA functional BP86, the hybrid functionals B3LYP and PBE0 along with Pople and Ahlrichs basis sets were initially tested for complex **7aa** as the benchmark system. Out of the used combinations, the PBE0/6-31G(d) level of theory gave the most reliable results and was therefore used in all presented calculations. Time-dependent calculations of the ground-state structures of all complexes were used to simulate the respective absorption spectra. The comparison of calculated and experimental spectrum is presented exemplarily for compound **7aa** in Figure 7 (see Figures S5–S14). The TD-DFT spectrum is in good

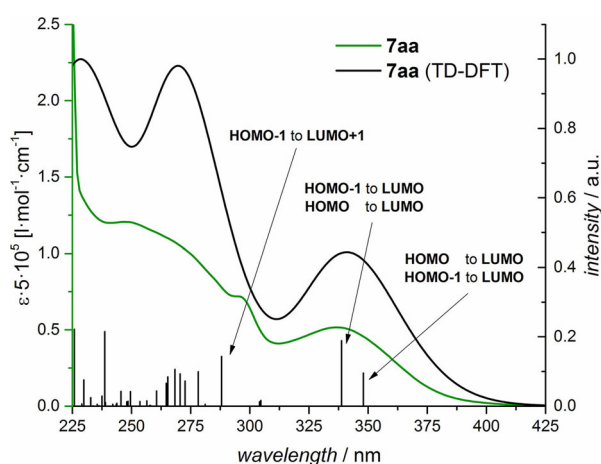


Figure 7. Exemplary comparison of experimental (green) and calculated (black, normalized). Calculated spectrum (0.333 eV half-width) and oscillator strengths given as obtained from calculation.

agreement with the experimentally obtained data. It describes two low-energy excitations between 330 and 350 nm, which are dominated by two transitions each from the highest occupied molecular orbitals (HOMO–1 and HOMO) to the lowest unoccupied molecular orbital (LUMO), respectively, with reversed order of contribution. For illustration, the respective natural transition orbitals (NTOs) were calculated and can be found in Figure 8 (top, middle). Both excitations occur from orbitals spread almost equally across the cyclometalating moiety of the heterocyclic and the acetylacetonate ligand, as well as the metal center, to orbitals almost exclusively centered on the *N*-heterocyclic ligand with significant contribution of the carbon-bound aryl fragment. This is in agreement with the shifts in the corresponding absorption band, observed for the bromine- and nitrile-substituted compounds, discussed earlier. The characteristic band around 295 nm correlates to a HOMO–1→LUMO+1 dominated excitation to the acetylacetonate fragment (Figure 8, bottom) which matches the unaltered position of the band in the experimental spectra for the acetylacetonate complexes (Figure 4). In the case of the aryl-substi-

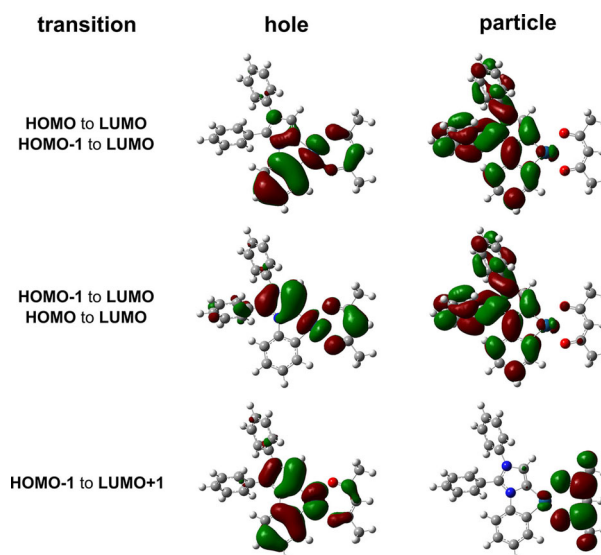


Figure 8. NTO analysis (isoval = 0.04) of compound **7aa** for the transitions highlighted in Figure 7.

tuted β -diketonate ligands, the particle orbitals are spread across the mesityl and duryl fragments (see Figure S7), as well, which thereby influence this transition.

The ground and triplet state structures for all platinum(II) complexes were optimized and the results are given exemplarily for compound **7aa** in Figure 9. While the ground state structure with a singlet electron configuration (Figure 9, left) closely resembles the molecular geometry obtained by X-ray diffraction, the optimized structure in the triplet state shows significant differences. Upon excitation, DFT predicts a significant distortion of the molecule (Figure 9, right). The results of this geometry optimization could be reproduced with all benchmarked functional/basis set combinations (see Figures S15–S17). The platinum(II) complex appears to bend with the imidazole ring, and the aryl fragments bound to it, twisting out of the coordination plane. This distortion allows for the

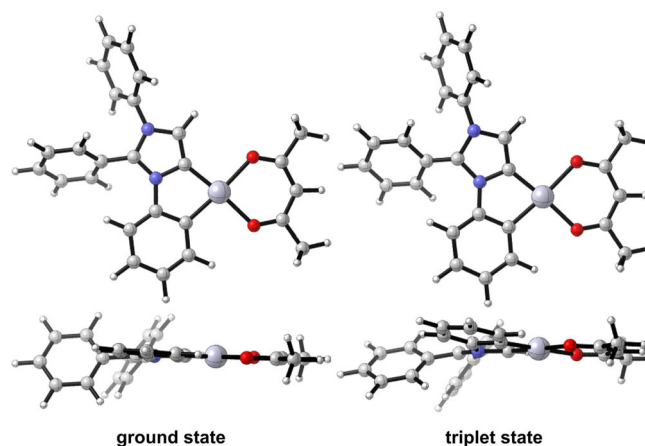


Figure 9. Optimized geometries for compound **7aa** in the ground state (left) and in the triplet state (right). Side views (bottom) relative to the imidazole ring.

carbon-bound phenyl ring to decrease the dihedral angle towards the imidazole ring and thereby increases its electronic influence on the delocalized system. This can be visualized by plotting the frontier molecular orbitals (FMOs) for the optimized ground and the spin density of the triplet state structures (Figure 10). While the LUMO is spread almost equally

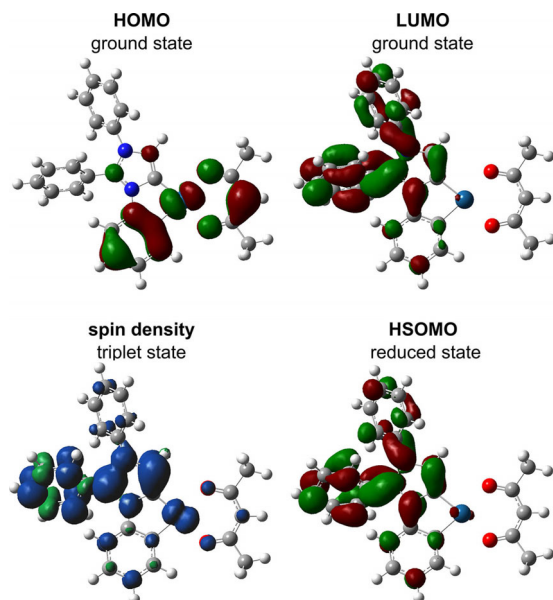


Figure 10. Calculated frontier molecular orbitals (isoval = 0.03) and spin density (density = 0.002) for **7aa**.

across the two non-coordinating aryl moieties of the *N*-heterocyclic ligand, the carbon-bound aryl fragment influences the spin density of the triplet state to a significantly greater extent. This allows for the electronic modifications introduced by the bromine and nitrile groups to effectively influence the emission properties of the platinum(II) complexes. However, due to the contribution of the carbon-bound aryl fragment to the LUMO, these effects are also visible in the optical bandgaps of the respective compounds. The energy difference between HOMO and LUMO can be estimated by determining the onset of the lowest energy absorption band in the UV/Vis spectra. The results are given in Table 2 and show a clear trend. The energy difference decreases when going from the unsubstituted compounds **7aa–7ac** to the bromine (**7ba–7bc**) and nitrile

(**7ac–7cc**) functionalized complexes. This tendency is also reproduced in E_g (TD-DFT)—estimating the optical bandgap from time-dependent calculations—and the HOMO–LUMO gap obtained from the optimized ground state structures.

Cyclic voltammetry

To verify these results by additional experimental data, cyclic voltammetry experiments were conducted, providing insights into the contributions of the ligands to the FMOs (Figure 11 and Supporting Information Figures S18–S27). Of particular interest are the observed reductive events, since DFT calculations and previous experiments^[15b] could show that the HSOMO of the first reduction (Figure 10) closely resembles the LUMO of the ground state and also the HSOMO of the excited state. The geometry of the radical monoanion can be calculated by DFT and, interestingly, shows the same geometry distortion as was observed for the optimized triplet state structures (see Figure S28), which is in agreement with the behaviour of earlier reported cyclometalated platinum(II) compounds.^[15b] The onset potential for the first irreversible reduction is recorded at $E(\text{red})_{\text{onset}} = -2.54$ V (Table 2) for complex **6aa** and is reduced by approximately 0.2 V for **7aa** (–2.34 V). This is in accordance with the calculated HSOMO of the radical anion. The non-coordinating *N*-phenyl moiety of the *N*-heterocyclic ligand aids in

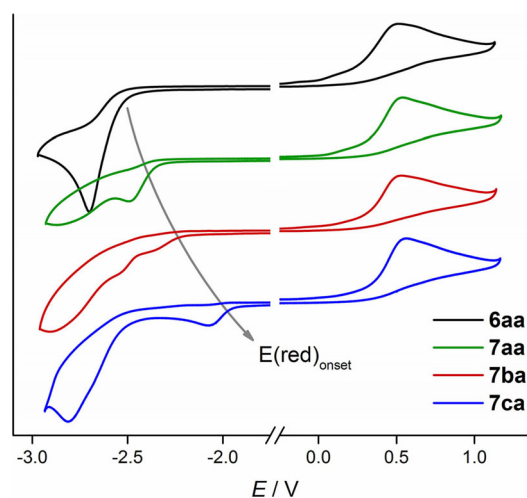


Figure 11. CV spectra of selected complexes. Recorded in DMF solution, referenced internally against Fc/Fc^+ .

Table 2. Comparison of experimentally determined and calculated values for the optical band HOMO–LUMO gap for all title compounds. Electrochemical data obtained from cyclic voltammetry experiments.

	6aa	7aa	7ab	7ac	7ba	7bb	7bc	7ca	7cb	7cc
$E_g(\text{exp})$ [eV] ^[a]	3.3	3.2	3.2	3.2	3.1	3.1	3.1	2.9	2.9	2.9
$E_g(\text{TD-DFT})$ [eV] ^[b]	3.7	3.6	3.6	3.6	3.4	3.4	3.4	3.1	3.1	3.1
$\Delta E(\text{H-L})$ [eV] ^[c]	3.8	3.8	3.9	3.9	3.7	3.7	3.7	3.1	3.2	3.2
$E(\text{red})_{\text{onset}}$ [V] ^[d]	–2.54	–2.34	–2.38	–2.39	–2.21	–2.22	–2.23	–1.94	–1.98	–1.97

[a] Optical band gap E_g estimated from absorption onset and photon energy equation. [b] Optical band gap E_g calculated from the lowest energy transition obtained from time-dependent calculations. [c] HOMO–LUMO energy difference calculated from the FMO eigenvalues obtained in the geometry optimization. [d] Cyclic voltammetry data referenced internally vs. Fc/Fc^+ .

stabilizing the surplus electron in the latter complex. Expectedly, the reduction potentials for the bromine and nitrile functionalized complexes **7ba** (−2.21 V) and **7ca** (−1.94 V) further decrease according to the electron-withdrawing ability of these substituents. The additional aryl fragments in the mesacac and duracac complexes do not contribute to the HSOMO and therefore $E(\text{red})_{\text{onset}}$ stays very much similar to that of the respective acetylacetonate complexes.

Conclusions

$C^{\wedge}C^*$ cyclometalated complexes of iridium and platinum, as the most relevant transition metals for phosphorescent complexes, with classically bound imidazole-based ligands have been synthetically available for years and their photophysical properties studied in detail. Their abnormally bound analogues on the other hand, remained elusive, with only very few structures reported for iridium^[23] and platinum complexes^[16a,b] only being mentioned in patents. The conducted studies focused only on the possible application of the aNHC complexes as homogenous catalysts.

In this manuscript we report the synthesis of the first platinum(II) complexes with bidentate $C^{\wedge}C^*$ cyclometalated aNHC ligands and present a systematic study of their photophysical properties. Preparation of the carbene ligand precursors was achieved starting from commercially available compounds, allowing for steric and electronic variations in the motif. The proposed structures were confirmed by NMR experiments as well as solid-state structures, which clearly show the presence of abnormal *N*-heterocyclic ligands. The photophysical properties of the presented complexes were studied in detail by UV/Vis spectroscopy and photoluminescence measurements. The complexes showed strong emissions in the green to yellow region of the visible spectrum, with photoluminescence quantum yields ranging from 40–69% and emission lifetimes from 27 to 57 μs . The unstructured band shape of these emissions at room temperature was retained even at 77 K. The photoluminescence measurements were accompanied by DFT calculations and cyclic voltammetry (CV) experiments, which helped to elucidate the contributions of the molecular moieties to the emissive process. The ground state HOMO is spread evenly across the cyclometalating moieties of the *N*-heterocyclic and β -diketonate ligands, as well as, the platinum center, while the excited triplet state is strongly influenced by the carbon-bound aryl fragment of the aNHC ligand. Taking into account all presented experimental and theoretical data, we can propose a strongly metal-perturbed intra-ligand/metal-to-ligand charge-transfer (ILCT/MLCT) process in the emission. The strong phosphorescence at room temperature and long-lived excited state suggest an application of the presented complexes as sensitizing molecules or photocatalysts.

Experimental Section

General considerations: All amidines and platinum complexes were synthesized in flame dried Schlenk flasks under argon atmosphere. Solvents of at least 99.0% purity were used in all reactions

in this study. Dimethylformamide (DMF) was dried using standard techniques and stored over molecular sieve (3 Å). Dichloro(cycloocta-1,5-diene)platinum(II) was prepared according to a modified literature procedure.^[24] Bis-1,3-(2,4,6-trimethyl-phenyl)propan-1,3-dione and bis-1,3-(2,3,5,6-tetramethylphenyl)-propan-1,3-dione were prepared according to a modified literature procedure.^[25] All other chemicals were obtained from common suppliers and used without further purification. ¹H, ¹³C, ¹⁹F and ¹⁹⁵Pt spectra were acquired on Bruker NMR Avance 300, Bruker DRX 500 and Bruker Avance 600 NMR spectrometers. ¹H and ¹³C spectra were referenced internally (¹H: 7.26 ppm, ¹³C 77.16 ppm for CDCl₃; ¹H: 2.50 ppm, ¹³C 39.43 ppm for [D₆]DMSO). ¹⁹⁵Pt spectra were referenced externally by using potassium tetrachloroplatinate(II) in D₂O (PtCl₄²⁻: −1617.2 ppm). Chemical shifts are given in ppm, coupling constants *J* in Hz. Elemental analyses were performed by the microanalytical laboratory of our institute on a Hekatech EA 3000 Euro Vector elemental analyzer. Melting points were determined by using a Wagner and Munz PolyTherm A system and are not corrected.

Photoluminescence measurements: The 2 wt% emitter films were prepared by doctor blading a solution of an emitter in a 10 wt% PMMA solution in dichloromethane on a quartz substrate with a 60 μm doctor blade. The film was dried and the emission was measured under nitrogen atmosphere. Room temperature experiments in degassed dichloromethane solution were carried out at a concentration of $5 \times 10^{-5} \text{ mol L}^{-1}$. Solutions for the low temperature measurements at 77 K were prepared by dissolving the emitter in degassed 2-MeTHF to give a concentration of $4.5 \times 10^{-5} \text{ mol L}^{-1}$. The frozen samples in quartz cuvettes were inserted in a quartz finger dewar containing liquid nitrogen. Excitation was conducted in a wavelength range of 250–400 nm (Xe lamp with a monochromator), and the emission was detected with a calibrated quantum yield detection system (Hamamatsu, model C11 347-01). The phosphorescence decay was measured with an Edinburgh Instruments mini- τ by excitation with pulses of an EPLED (360 nm, 20 kHz) and time-resolved photon counting (TCSPC). Absorption spectra were measured on a PerkinElmer Lambda 365 UV/Vis spectrometer in dichloromethane solutions with an analyte concentration of $5 \times 10^{-5} \text{ mol L}^{-1}$.

Electrochemistry: Cyclic voltammetry experiments were carried out using a Biologic SP-150 potentiostat in degassed, dry DMF solutions, employing a platinum wire counter electrode, a glassy carbon working electrode and a Ag/Ag⁺ pseudo reference electrode. All complexes were measured as 0.5 mM solutions along with 0.1 M supporting electrolyte (N(nBu)₄ClO₄) at a sweep rate of 50 mV s^{−1}. All measurements were internally referenced against Fc/Fc⁺.

Computational details: The Gaussian16^[26] package was used to perform all quantum chemical calculations employing the hybrid functionals B3LYP^[27] and PBE0,^[28] as well as, the pure functional BP86^[28a,b,29] together with 6-31G(d)^[30] and def2-SVP^[31] basis sets. Platinum was described by LANL2DZ ECP and basis set.^[32] All given structures were verified as true minima by vibrational frequency analysis and the absence of negative eigenvalues. UV/Vis spectra and electronic transitions were calculated using TD-DFT methods (singlet, nstates=50, CPCM, solvent=dichloromethane) as implemented in the Gaussian16 package. Calculated geometries were visualized with CYLview^[33] and GaussView.^[34]

Synthesis and characterization: A detailed description of the synthetic procedures is given exemplarily for each class of compounds. Please refer to the Supporting Information for the synthesis and analytical data of the analogously prepared compounds.

Compound 2a: In a 50 mL Schlenk round-bottom flask, 0.360 g (15 mmol, 1.5 equiv) sodium hydride is suspended in 5 mL of dry DMSO. The mixture was cooled using an ice bath while 1.031 g (10 mmol) benzonitrile and 1.118 g (12 mmol, 1.2 equiv) aniline are added via syringe. The reaction was stirred for one hour at this temperature and then allowed to warm to room temperature while stirring overnight. Deionized water was slowly added while the mixture is again cooled in an ice bath and the precipitate collected and washed with an excess of deionized water. After drying in vacuo, the solid was triturated with isohexanes and again dried under reduced pressure (1.42 g, 72%). M.p. 103 °C. ¹H NMR in CDCl₃ (300 MHz) δ 7.84 (d, *J* = 6.7 Hz, 2H, CH_{arom}), 7.55–7.40 (m, 3H, CH_{arom}), 7.40–7.30 (m, 2H, CH_{arom}), 7.14–6.94 (m, 3H, CH_{arom}), 4.94 (brs, 2H, NH₂). ¹³C NMR in CDCl₃ (75 MHz) δ 130.9 (CH_{arom}), 129.7 (CH_{arom}), 128.8 (CH_{arom}), 127.1 (CH_{arom}), 123.5 (CH_{arom}), 122.0 (CH_{arom}). Anal. calcd for C₁₃H₁₂N₂: C 79.56%; H 6.16%; N 14.27%. Found: C 79.57%; H 6.39%; N 14.17%.

Compound 3a: In a 100 mL round-bottom flask, 2.944 g (15 mmol) of compound **2a** and 4.710 g (30 mmol, 2 equiv) of a chloroacetaldehyde in water (*c* = 50%) are dissolved in 40 mL chloroform. The mixture is refluxed for 24 hours and subsequently quenched with a saturated sodium bicarbonate solution in water. The aqueous phase is extracted with dichloromethane. After drying the organic phase over magnesium sulfate, the product is isolated by column chromatography with the eluent ethyl acetate (2.21 g 68%). M.p. 73 °C. ¹H NMR in CDCl₃ (300 MHz) δ 7.44–7.37 (m, 5H, CH_{arom}), 7.30–7.21 (m, 6H, CH_{arom}), 7.17 (d, *J* = 1.3 Hz, 1H, CH_{arom}). ¹³C NMR in CDCl₃ (75 MHz) δ 146.7 (C=O), 138.5 (C=O), 130.1 (C=C), 129.6 (CH_{arom}), 128.8 (CH_{arom}), 128.7 (CH_{arom}), 128.6 (CH_{arom}), 128.3 (2 CH_{arom}), 126.0 (CH_{arom}), 123.0 (CH_{arom}). Anal. calcd for C₁₅H₁₂N₂: C 81.79%; H 5.49%; N 12.72%. Found: C 81.75%; H 5.62%; N 12.46%.

Compound 4a: In a sealed tube, 1.101 g (5 mmol) of compound **3a** and 1.434 g (10 mmol, 2 equiv) methyl iodide are dissolved in 3 mL THF. The mixture is heated to 110 °C for 24 hours. The precipitate is collected, washed with small volumes of THF and diethyl ether and subsequently dried in vacuo (1.50 g, 83%). M.p. 243 °C. ¹H NMR in [D₆]DMSO (300 MHz) δ 8.18 (d, *J* = 2.1 Hz, 1H, CH_{arom}), 8.12 (d, *J* = 2.1 Hz, 1H, CH_{arom}), 7.64–7.56 (m, 3H, CH_{arom}), 7.56–7.51 (m, 2H, CH_{arom}), 7.51–7.46 (m, 3H, CH_{arom}), 7.44–7.38 (m, 2H, CH_{arom}), 3.79 (s, 3H, NCH₃). ¹³C-NMR in [D₆]DMSO (75 MHz) δ 144.3 (C=O), 135.1 (C=C), 132.0 (CH_{arom}), 130.9 (CH_{arom}), 130.1 (CH_{arom}), 129.7 (CH_{arom}), 129.0 (CH_{arom}), 126.2 (CH_{arom}), 123.7 (CH_{arom}), 123.5 (CH_{arom}), 121.4 (C=C), 35.9 (NCH₃). Anal. calcd for C₁₆H₁₅IN₂: C 53.06%; H 4.17%; N 7.73%. Found: C 52.83%; H 3.81%; N 7.75%.

Compound 5a: In a Schlenk tube, 1.652 g (7.5 mmol) of compound **3a**, 3.311 g (9 mmol, 1.2 equiv) diphenyliodonium tetrafluoroborate and 0.075 g (0.38 mmol, 0.05 equiv) copper(II) acetate monohydrate are dissolved in 20 mL DMF. The mixture is heated to 100 °C for 18 hours. All volatiles are removed under reduced pressure and the product is crystallized from hot methanol. The precipitate is collected and washed with diethyl ether and dried in vacuo (2.55 g, 89%). M.p. 274 °C. ¹H NMR in [D₆]DMSO (300 MHz) δ 8.43 (s, 2H, CH_{arom}), 7.62–7.26 (m, 15H, CH_{arom}). ¹³C-NMR in [D₆]DMSO (75 MHz) δ 144.5 (C=O), 135.0 (C=C), 131.8 (CH_{arom}), 131.2 (CH_{arom}), 130.3 (CH_{arom}), 129.7 (CH_{arom}), 128.6 (CH_{arom}), 126.4 (CH_{arom}), 124.0 (CH_{arom}), 121.6 (C=C). Anal. calcd for: C₂₁H₁₇BF₄N₂: C 65.65%; H 4.46%; N 7.29%. Found: C 65.75%; H 4.74%; N 7.33%.

Compound 6aa: In a flame dried Schlenk tube, 0.580 g (1.6 mmol) of compound **4a** and 0.297 g (1.28 mmol, 0.8 equiv) silver(I) oxide are dissolved in 40 mL dry DMF and heated to 75 °C for 23 h. After adding 599 mg (1.6 mmol, 1 equiv) Pt(COD)Cl₂, the mixture is stirred at room temperature for three hours and subsequently heated to 130 °C for another 21 hours. The solution is cooled to

room temperature, 0.641 g (6.4 mmol, 4 equiv) acetylacetone and 0.885 g (6.4 mmol, 4 equiv) potassium carbonate are added and stirred at room temperature for 21 hours and afterwards at 100 °C for six hours. All volatiles are removed in vacuo and the residue is washed with ca. 40 mL of distilled water. The remaining solid is filtered, dried at 60 °C overnight and extracted with DCM. The product is purified by flash column chromatography with a gradient of isohexanes/ethyl acetate (2:1) to pure ethyl acetate. The compound is dissolved in DCM and run over a plug of Celite. After removal of all volatiles under reduced pressure, the analytically pure product is obtained after washing the solid with isohexanes and diethyl ether (3 × 5 mL each) and drying in vacuo. (155 mg, 18%). M.p. 253 °C. ¹H NMR in CDCl₃ (300 MHz) δ 7.82 (dd, *J* = 7.5, 1.4 Hz, 1H, PtCCH of N3-Ph), 7.74–7.57 (m, 3H, CH_{para/meta} of C2-Ph), 7.46 (dd, *J* = 10.9, 9.3 Hz, 2H, CH_{ortho} of C2-Ph), 7.00–6.80 (m, 2H, CH_{para} of N3-Ph & NCH), 6.63 (t, *J* = 7.2 Hz, 1H, CH_{meta} of N3-Ph), 6.18 (d, *J* = 8.0 Hz, 1H, CH_{ortho} of N3-Ph), 5.43 (s, 1H, COCH), 3.47 (s, 3H, NCH₃), 2.00 (s, 3H, COCH₃), 1.95 (s, 3H, COCH₃). ¹³C-NMR in CDCl₃ (75 MHz) δ 184.9 (C=O), 184.7 (C=O), 148.1 (C=C of N3-Ph), 139.5 (N₃CN), 133.0 (PtCCH of N3-Ph), 132.1 (PtCN), 131.9 (CH_{para} of C2-Ph), 130.5 (CH_{ortho} of C2-Ph), 129.9 (CH_{meta} of C2-Ph), 129.5 (PtCCH), 125.5 (CH_{para} of N3-Ph), 124.5 (C=C of C2-Ph), 122.4 (CH_{meta} of N3-Ph), 120.2 (NCH), 112.9 (CH_{ortho} of N3-Ph), 102.0 (COCH), 34.3 (NCH₃), 28.2 (COCH₃), 28.1 (COCH₃). ¹⁹⁵Pt NMR in CDCl₃ (64 MHz) δ –3369.4 (s). MS (ESI) *m/z* = 528.3 [M+H]⁺, 955.5 [2M+aca]⁺. Anal. calcd for C₂₁H₂₀N₂O₂Pt · 0.16 CH₂Cl₂: C 46.97%; H 3.79%; N 5.18%; Found: C 47.25%; H 3.48%; N 5.29%.

Compound 7aa: In a flame dried Schlenk tube, 0.615 g (1.6 mmol) of compound **5a** and 0.185 g (0.8 mmol, 0.5 equiv) silver(I) oxide are dissolved in 40 mL dry DMF and heated to 75 °C for 23 h. After adding 0.599 g (1.6 mmol, 1 equiv) Pt(COD)Cl₂, the mixture is stirred at room temperature for three hours and subsequently heated to 130 °C for another 21 hours. The solution is cooled to room temperature, 0.320 g (3.2 mmol, 2 equiv) acetylacetone and 0.442 g (3.2 mmol, 2 equiv) potassium carbonate are added and stirred at room temperature for 21 hours and afterwards at 100 °C for six hours. All volatiles are removed in vacuo and the residue is washed with ca. 40 mL of distilled water. The remaining solid is filtered, dried at 60 °C overnight and extracted with DCM. The product is purified by flash column chromatography with a gradient of isohexanes/ethyl acetate (3:1) to isohexanes/ethyl acetate (2:1). After removal of all volatiles under reduced pressure, the analytically pure product is obtained after washing the solid with isohexanes and diethyl ether (3 × 5 mL each) and drying in vacuo. (463 mg, 49%). M.p. 300 °C. ¹H NMR in CDCl₃ (600 MHz) δ 7.87 (dd, *J* = 7.6, 1.5 Hz, 1H, PtCCH of N3-Ph), 7.56–7.51 (m, 1H, CH_{para} of C2-Ph), 7.50–7.43 (m, 2H, CH_{meta} of C2-Ph), 7.39–7.36 (m, 2H, CH_{ortho} of C2-Ph), 7.36–7.31 (m, 3H, CH_{para/meta} of N1-Ph), 7.20–7.16 (m, 2H, CH_{ortho} of N1-Ph), 7.11 (s, 1H, NCH), 6.97 (td, *J* = 7.4, 1.2 Hz, 1H, CH_{para} of N3-Ph), 6.69–6.64 (m, 1H, CH_{meta} of N3-Ph), 6.31 (dd, *J* = 8.1, 1.2 Hz, 1H, CH_{ortho} of N3-Ph), 5.44 (s, 1H, COCH), 2.02 (s, 3H, COCH₃), 1.94 (s, 3H, COCH₃). ¹³C-NMR in CDCl₃ (151 MHz) δ 185.0 (C=O), 184.8 (C=O), 147.9 (C=C of N3-Ph), 139.4 (N₃CN), 136.2 (C=C of N1-Ph), 133.1 (PtCCH of N3-Ph), 132.3 (PtCN), 131.6 (CH_{para} of C2-Ph), 131.0 (CH_{ortho} of C2-Ph), 130.1 (PtCCH of N3-Ph), 129.6 (CH_{meta} of C2-Ph), 129.5 (CH_{meta} of N1-Ph), 129.2 (CH_{para} of N1-Ph), 126.0 (CH_{ortho} of N1-Ph), 125.8 (CH_{para} of N3-Ph), 124.5 (C=C of C2-Ar), 122.5 (CH_{meta} of N3-Ph), 120.9 (NCH), 113.6 (CH_{ortho} of N3-Ph), 102.0 (COCH), 28.2 (COCH₃), 28.0 (COCH₃). ¹⁹⁵Pt NMR in CDCl₃ (64 MHz) δ –3371.6 (s). MS (ESI) *m/z* = 590.3 [M+H]⁺, 1079.5 [2M+H]⁺. Anal. calcd for C₂₆H₂₂N₂O₂Pt: C 52.97%; H 3.76%; N 4.75%. Found: C 52.65%; H 3.57%; N 4.75%.

Acknowledgements

We are very grateful to the ZIH Dresden for the allocation of computational time on their high performance computing system. J.S. would like to thank the Studienstiftung des Deutschen Volkes for funding.

Conflict of interest

The authors declare no conflict of interest.

Keywords: abnormal N-heterocyclic carbenes • mesoionic • OLEDs • phosphorescence • platinum

- [1] A. J. Arduengo III, R. L. Harlow, M. Kline, *J. Am. Chem. Soc.* **1991**, *113*, 361–363.
- [2] a) K. Öfele, *J. Organomet. Chem.* **1968**, *12*, P42–P43; b) H. W. Wanzlick, H. J. Schönherr, *Angew. Chem. Int. Ed. Engl.* **1968**, *7*, 141–142; *Angew. Chem.* **1968**, *80*, 154–154.
- [3] C. M. Crudden, D. P. Allen, *Coord. Chem. Rev.* **2004**, *248*, 2247–2273.
- [4] a) Y. Chi, P.-T. Chou, *Chem. Soc. Rev.* **2010**, *39*, 638–655; b) J. Nitsch, F. Lacombe, A. Lorbach, A. Eichhorn, F. Cisnetti, A. Steffen, *Chem. Commun.* **2016**, *52*, 2932–2935; c) T. Fleetham, G. Li, L. Wen, J. Li, *Adv. Mater.* **2014**, *26*, 7116–7121; d) V. W.-W. Yam, K. M.-C. Wong, *Chem. Commun.* **2011**, *47*, 11579–11592; e) D. N. Kozhevnikov, V. N. Kozhevnikov, M. Z. Shafikov, A. M. Prokhorov, D. W. Bruce, J. A. Gareth Williams, *Inorg. Chem.* **2011**, *50*, 3804–3815; f) Z. M. Hudson, B. A. Blight, S. Wang, *Org. Lett.* **2012**, *14*, 1700–1703; g) A. Diez, E. Lalinde, M. T. Moreno, S. Ruiz, *Organometallics* **2016**, *35*, 1735–1746.
- [5] H. Yersin, W. J. Finkenzeller, *Highly Efficient OLEDs with Phosphorescent Materials* (Ed.: H. Yersin), Wiley-VCH, Weinheim, **2008**, pp. 1–97.
- [6] a) H. Yersin, *Top. Curr. Chem.* **2004**, *241*, 1–26; b) H. Yersin, A. F. Rausch, R. Czerwieńiec, T. Hofbeck, T. Fischer, *Coord. Chem. Rev.* **2011**, *255*, 2622–2652.
- [7] a) H. Xu, R. Chen, Q. Sun, W. Lai, Q. Su, W. Huang, X. Liu, *Chem. Soc. Rev.* **2014**, *43*, 3259–3302; b) A. Endo, K. Suzuki, T. Yoshihara, S. Tobita, M. Yahiro, C. Adachi, *Chem. Phys. Lett.* **2008**, *460*, 155–157; c) W. C. H. Choy, W. K. Chan, Y. Yuan, *Adv. Mater.* **2014**, *26*, 5368–5399; d) C. Adachi, M. A. Baldo, M. E. Thompson, S. R. Forrest, *J. Appl. Phys.* **2001**, *90*, 5048–5051; e) T. Sajoto, P. I. Djurovich, A. Tamayo, M. Yousufuddin, R. Bau, M. E. Thompson, R. J. Holmes, S. R. Forrest, *Inorg. Chem.* **2005**, *44*, 7992–8003; f) C.-H. Yang, J. Beltran, V. Lemaire, J. Cornil, D. Hartmann, W. Sarfert, R. Froehlich, C. Bizzarri, L. De Cola, *Inorg. Chem.* **2010**, *49*, 9891–9901; g) C. Yang, *Chem. Sci.* **2016**, *7*, 3123–3136; h) T.-Y. Li, X. Liang, L. Zhou, C. Wu, S. Zhang, X. Liu, G.-Z. Lu, L.-S. Xue, Y.-X. Zheng, J.-L. Zuo, *Inorg. Chem.* **2015**, *54*, 161–173; i) F. Kessler, *Dalton Trans.* **2012**, *41*, 180–191; j) F. Zhang, L. Duan, J. Qiao, G. Dong, L. Wang, Y. Qiu, *Org. Electron.* **2012**, *13*, 1277–1288; k) R. Liu, S. Zhu, H. Shi, J. Hu, M. Shu, J. Liu, H. Zhu, *Inorg. Chem. Commun.* **2016**, *74*, 26–30.
- [8] a) T. Fleetham, G. Li, J. Li, *Adv. Mater.* **2017**, *29*, 1601861–1601861 and references therein; b) M. Elie, J. L. Renaud, S. Gaillard, *Polyhedron* **2018**, *140*, 158–168 and references therein; c) G. L. Petretto, M. Wang, A. Zucca, J. P. Rourke, *Dalton Trans.* **2010**, *39*, 7822–7825; d) K. Li, X. Guan, C.-W. Ma, W. Lu, Y. Chen, C.-M. Che, *Chem. Commun.* **2011**, *47*, 9075–9077; e) T. Fleetham, Z. Wang, J. Li, *Org. Electron.* **2012**, *13*, 1430–1435; f) R. Visbal, M. C. Gimeno, *Chem. Soc. Rev.* **2014**, *43*, 3551–3574 and references therein; g) S.-B. Ko, H.-J. Park, S. Gong, X. Wang, Z.-H. Lu, S. Wang, *Dalton Trans.* **2015**, *44*, 8433–8443; h) K. Li, G. Cheng, C. Ma, X. Guan, W.-M. Kwok, Y. Chen, W. Lu, C.-M. Che, *Chem. Sci.* **2013**, *4*, 2630–2644; i) S. Fuentès, A. J. Chueca, M. Peralvarez, P. Borja, M. Torrell, J. Carreras, V. Sicilia, *ACS Appl. Mater. Interfaces* **2016**, *8*, 16160–16169; j) Z. M. Hudson, C. Sun, M. G. Helander, Y.-L. Chang, Z.-H. Lu, S. Wang, *J. Am. Chem. Soc.* **2012**, *134*, 13930–13933; k) M. Bachmann, D. Suter, O. Blacque, K. Venkatesan, *Inorg. Chem.* **2016**, *55*, 4733–4745; l) S. Fuentès, H. García, M. Peralvarez, W. Hertog, J. Carreras, V. Sicilia, *Chem. Eur. J.* **2015**, *21*, 1620–1631.
- [9] a) Y. Unger, D. Meyer, O. Molt, C. Schildknecht, I. Muenster, G. Wagenblast, T. Strassner, *Angew. Chem. Int. Ed.* **2010**, *49*, 10214–10216; *Angew. Chem.* **2010**, *122*, 10412–10414; b) T. Strassner, *Acc. Chem. Res.* **2016**, *49*, 2680–2689 and references therein.
- [10] a) S. Fuentès, A. J. Chueca, L. Arnal, A. Martin, U. Giovanella, C. Botta, V. Sicilia, *Inorg. Chem.* **2017**, *56*, 4829–4839; b) J. Brooks, Y. Babayan, S. Lamansky, P. I. Djurovich, I. Tsyba, R. Bau, M. E. Thompson, *Inorg. Chem.* **2002**, *41*, 3055–3066; c) A. R. Naziruddin, C.-S. Lee, W.-J. Lin, B.-J. Sun, K.-H. Chao, A. H. H. Chang, W.-S. Hwang, *Dalton Trans.* **2016**, *45*, 5848–5859; d) B. Schulze, C. Friebe, M. Jaeger, H. Goerls, E. Birkner, A. Winter, U. S. Schubert, *Organometallics* **2018**, *37*, 145–155.
- [11] a) S. Gründemann, A. Kovacevic, M. Albrecht, J. W. Faller, R. H. Crabtree, *J. Am. Chem. Soc.* **2002**, *124*, 10473–10481; b) S. Gruendemann, A. Kovacevic, M. Albrecht, J. W. Faller Robert, H. Crabtree, *Chem. Commun.* **2001**, 2274–2275.
- [12] a) M. Albrecht, *Chem. Commun.* **2008**, 3601–3610; b) R. H. Crabtree, *Coord. Chem. Rev.* **2013**, *257*, 755–766; c) O. Schuster, L. Yang, H. G. Raubenheimer, M. Albrecht, *Chem. Rev.* **2009**, *109*, 3445–3478.
- [13] a) M. Alcarazo, S. J. Roseblade, A. R. Cowley, R. Fernández, J. M. Brown, J. M. Lassaletta, *J. Am. Chem. Soc.* **2005**, *127*, 3290–3291; b) A. R. Chianese, A. Kovacevic, B. M. Zeglis, J. W. Faller, R. H. Crabtree, *Organometallics* **2004**, *23*, 2461–2468; c) G. Song, Y. Zhang, X. Li, *Organometallics* **2008**, *27*, 1936–1943.
- [14] D. Yuan, H. V. Huynh, *Organometallics* **2012**, *31*, 405–412.
- [15] a) J. Soellner, M. Tenne, G. Wagenblast, T. Strassner, *Chem. Eur. J.* **2016**, *22*, 9914–9918; b) J. Soellner, T. Strassner, *Chem. Eur. J.* **2018**, *24*, 5584–5590; c) A. Baschieri, F. Monti, E. Matteucci, A. Mazzanti, A. Barbieri, N. Armaroli, L. Sambri, *Inorg. Chem.* **2016**, *55*, 7912–7919; d) P. Châbera, *Nature* **2017**, *543*, 695–699; e) L. Hettmanczyk, S. J. P. Spall, S. Klensk, M. van der Meer, S. Hohloch, J. A. Weinstein, B. Sarkar, *Eur. J. Inorg. Chem.* **2017**, *14*, 2112–2121; f) V. Leigh, W. Ghattas, R. Lalrempuia, H. Muller-Bunz, M. T. Pryce, M. Albrecht, *Inorg. Chem.* **2013**, *52*, 5395–5402; g) M. Navarro, S. Wang, H. Muller-Bunz, G. Redmond, P. Farras, M. Albrecht, *Organometallics* **2017**, *36*, 1469–1478.
- [16] a) T. K. Hollis, X. Zhang, (University of Mississippi, USA), WO2011050003A2, **2011**; b) T. K. Hollis, X. Zhang, (University of Mississippi, USA), US9029804B2, **2015**; c) D. Bacciu, K. J. Cavell, I. A. Fallis, L.-I. Ooi, *Angew. Chem. Int. Ed.* **2005**, *44*, 5282–5284; *Angew. Chem.* **2005**, *117*, 5416–5418; d) G. C. Fortman, N. M. Scott, A. Linden, E. D. Stevens, R. Dorta, S. P. Nolan, *Chem. Commun.* **2010**, *46*, 1050–1052; e) H. Jin, T. T. Y. Tan, F. E. Hahn, *Angew. Chem. Int. Ed.* **2015**, *54*, 13811–13815; *Angew. Chem.* **2015**, *127*, 14016–14020; f) V. Khlebnikov, M. Heckenroth, H. Mueller-Bunz, M. Albrecht, *Dalton Trans.* **2013**, *42*, 4197–4207; g) Q. Ge, B. Li, H. Song, B. Wang, *Org. Biomol. Chem.* **2015**, *13*, 7695–7710; h) D. Ghorai, J. Choudhury, *ACS Catal.* **2015**, *5*, 2692–2696; i) P. K. Hota, G. Vijaykumar, A. Pariyar, S. C. Sau, T. K. Sen, S. K. Mandal, *Adv. Synth. Catal.* **2015**, *357*, 3162–3170; j) R. Li, Y. Hu, R. Liu, R. Hu, B. Li, B. Wang, *Adv. Synth. Catal.* **2015**, *357*, 3885–3892; k) J. Ahmed, S. C. Sau, P. Sreejyothi, P. K. Hota, P. K. Vardhanapu, G. Vijaykumar, S. K. Mandal, *Eur. J. Org. Chem.* **2017**, *5*, 1004–1011; l) P. K. Hota, A. Jose, S. K. Mandal, *Organometallics* **2017**, *36*, 4422–4431; m) T. Mondal, S. De, B. Maity, D. Koley, *Chem. Eur. J.* **2016**, *22*, 15778–15790; n) S. C. Sau, S. Santra, T. K. Sen, S. K. Mandal, D. Koley, *Chem. Commun.* **2012**, *48*, 555–557.
- [17] A. R. Chianese, B. M. Zeglis, R. H. Crabtree, *Chem. Commun.* **2004**, 2176–2177.
- [18] J. Huang, Y. He, Y. Wang, Q. Zhu, *Chem. Eur. J.* **2012**, *18*, 13964–13967.
- [19] S. Okamoto, H. Ishikawa, Y. Shibata, Y.-i. Suhara, *Tetrahedron Lett.* **2010**, *51*, 5704–5707.
- [20] S. Li, J. Tang, Y. Zhao, R. Jiang, T. Wang, G. Gao, J. You, *Chem. Commun.* **2017**, *53*, 3489–3492.
- [21] a) T. Lv, Z. Wang, J. You, J. Lan, G. Gao, *J. Org. Chem.* **2013**, *78*, 5723–5730; b) H. Peters, *J. Chem. Soc. Trans.* **1902**, *81*, 1350–1361.
- [22] A. Tronnier, U. Heinemeyer, S. Metz, G. Wagenblast, I. Muenster, T. Strassner, *J. Mater. Chem. C* **2015**, *3*, 1680–1693.
- [23] a) Y. D. Bidal, O. Santoro, M. Melaimi, D. B. Cordes, A. M. Z. Slawin, G. Bertrand, C. S. J. Cazin, *Chem. Eur. J.* **2016**, *22*, 9404–9409; b) W. Zuo, P. Braunstein, *Dalton Trans.* **2012**, *41*, 636–643; c) W. Zuo, P. Braunstein, *Organometallics* **2012**, *31*, 2606–2615; d) G. Ung, G. Bertrand, *Chem. Eur. J.* **2011**, *17*, 8269–8272.
- [24] D. Drew, J. R. Doyle, *Inorganic Syntheses* **1990**, *28*, Wiley, New York, 346–349.

- [25] C. Zhang, P. Yang, Y. Yang, X. Huang, X.-J. Yang, B. Wu, *Synth. Commun.* **2008**, *38*, 2349–2356.
- [26] M. J. Frisch, et al., *Gaussian 16 Rev. B.01*, Wallingford, CT, **2016**.
- [27] a) A. D. Becke, *J. Chem. Phys.* **1993**, *98*, 5648–5652; b) C. Lee, W. Yang, R. G. Parr, *Phys. Rev. B Condens. Matter* **1988**, *37*, 785–789; c) S. H. Vosko, L. Wilk, M. Nusair, *Can. J. Phys.* **1980**, *58*, 1200–1211; d) P. J. Stephens, F. J. Devlin, C. F. Chabalowski, M. J. Frisch, *J. Phys. Chem.* **1994**, *98*, 11623–11627; e) B. Miehlich, A. Savin, H. Stoll, H. Preuss, *Chem. Phys. Lett.* **1989**, *157*, 200–206.
- [28] a) J. P. Perdew, *Phys. Rev. B Condens Matter* **1986**, *33*, 8822–8824; b) J. P. Perdew, *Phys. Rev. B Condens Matter* **1986**, *34*, 7406; c) C. Adamo, V. Barone, *J. Chem. Phys.* **1999**, *110*, 6158–6170.
- [29] A. D. Becke, *Phys. Rev. A Gen. Phys.* **1988**, *38*, 3098–3100.
- [30] a) R. Ditchfield, W. J. Hehre, J. A. Pople, *J. Chem. Phys.* **1971**, *54*, 724–728; b) W. J. Hehre, R. Ditchfield, J. A. Pople, *J. Chem. Phys.* **1972**, *56*, 2257–2261; c) V. A. Rassolov, J. A. Pople, M. A. Ratner, T. L. Windus, *J. Chem. Phys.* **1998**, *109*, 1223–1229; d) V. A. Rassolov, M. A. Ratner, J. A. Pople, P. C. Redfern, L. A. Curtiss, *J. Comput. Chem.* **2001**, *22*, 976–984; e) P. C. Hariharan, J. A. Pople, *Chem. Phys. Lett.* **1972**, *16*, 217–219; f) P. C. Hariharan, J. A. Pople, *Mol. Phys.* **1974**, *27*, 209–214; g) P. C. Hariharan, J. A. Pople, *Theor. Chim. Acta* **1973**, *28*, 213–222.
- [31] F. Weigend, R. Ahlrichs, *Phys. Chem. Chem. Phys.* **2005**, *7*, 3297–3305.
- [32] a) P. J. Hay, W. R. Wadt, *J. Chem. Phys.* **1985**, *82*, 270–283; b) W. R. Wadt, P. J. Hay, *J. Chem. Phys.* **1985**, *82*, 284–298; c) P. J. Hay, W. R. Wadt, *J. Chem. Phys.* **1985**, *82*, 299–310.
- [33] C. Y. Legault, *CYLVIEW 1.0.564 beta*, University of Shelbrooke, Canada, **2012**.
- [34] R. Dennington, T. A. Keith, J. M. Millam, *GaussView, Version 6*, Semichem Inc., Shawnee Mission, KS, **2016**.

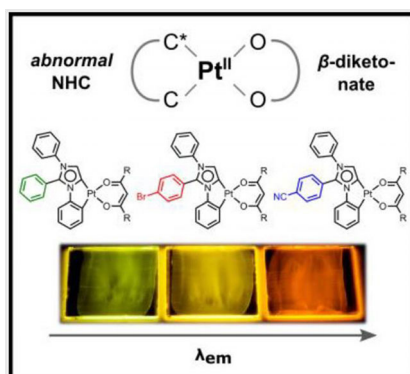
Manuscript received: May 29, 2018

Revised manuscript received: July 16, 2018

Version of record online: ■ ■ ■ ■, 0000

FULL PAPER

Photoluminescent platinum: The synthesis and characterization of the first platinum(II) complexes with C^ΛC* cyclometalated aNHC ligands is reported. The abnormal binding mode was unequivocally confirmed by solid-state structures and NMR experiments. Photoluminescence measurements, accompanied by DFT calculations and electrochemistry experiments, allowed insight into the emission characteristics of this class of compounds.



Photoluminescent Complexes

*J. Soellner, T. Strassner**



Phosphorescent Cyclometalated Platinum(II) aNHC Complexes

